# The Sun's Dynamic Influence on the Outer Heliosphere, the Heliosheath, and the Local Interstellar Medium

# The Sun's Dynamic Influence on the Outer Heliosphere, the Heliosheath, and the Local Interstellar Medium

**D S Intriligator[1], W Sun[1,2], T Detman[1], W D Miller[1], J Intriligator[1,3], M Dryer[1] W Webber[4], C Deehr[1,2] and G Gloeckler[5]**

[1]Carmel Research Center, Inc., Santa Monica, CA
[2]University of Alaska, Fairbanks, AK
[3]Bangor University, Bangor, Wales, UK
[4]New Mexico State University, Las Cruces, NM
[5]University of Michigan, Ann Arbor, MI

E-mail: devriei@aol.com

**Abstract**. The Sun has been observed for many years to be a dynamic influence in the heliosphere, and as the Voyager missions have continued long after achieving their original goals of observing the major planets they have provided the first *in situ* observations of the effects of solar activity in the heliosheath (HS), and the nearest portions of the local Interstellar Medium (LISM). Comparing these observations with models provides key insights. We employ two three-dimensional (3D) time-dependent models that simulate the propagation of shocks, other specific features, and the background solar wind throughout the heliosphere, starting with the solar background and solar event boundary conditions near the Sun at 2.5 Rs. The Hybrid Heliospheric Modeling System with Pickup Protons (HHMS-PI) is a 3D time-dependent Magnetohydrodynamic (MHD) simulation. HAFSS (HAF Solar Surface) is a 3D time-dependent kinematic simulation. Comparing our models with the observations indicates that solar effects are seen in the heliosphere, the HS, and the LISM in in-situ spacecraft measurements of plasma, magnetic field, energetic particles, cosmic rays, and plasma waves. There is quantitative agreement (at ACE, Ulysses, V1, V2) with data (e.g., solar wind, IMF, Ulysses SWICS pickup protons (PUPs)). Propagating shocks are slowed due to PUPs. The 3D locations of solar events and of various spacecraft are key to understanding the 3D propagation and timing of shocks, other specific features, and gradients throughout the heliosphere, HS, and LISM.

## 1. Introduction

It is a pleasure to recognize and honor Ed Stone and to acknowledge his many important contributions to space physics and astrophysics. Figure 1 shows three photos of Ed. ACE data and Voyager data are key for many aspects of our modeling and empirical analyses at Carmel Research Center, Inc.

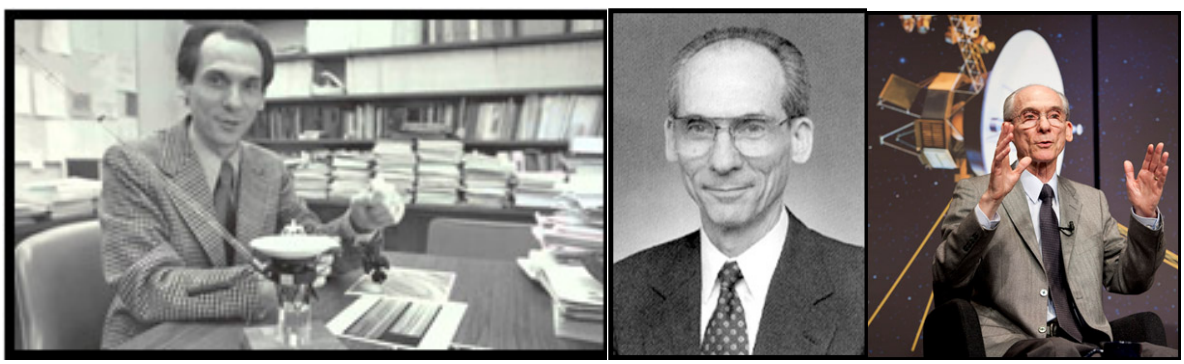

**Figure 1.** We are indebted to Ed Stone for his many important and significant contributions including those associated with ACE and Voyager. His tireless efforts have helped make available vast arrays of data that serve to extend our knowledge of the heliosphere and of the universe.

Figure 2a (the figure on the left) shows the two basic paths or components that are used to initiate both our HHMS-PI (Hybrid Heliospheric Modeling System with Pickup Protons), which is a three-dimensional (3D) time-dependent Magnetohydrodynamic (MHD) simulation; and HAFSS (HAF Solar Surface), which is a 3D time-dependent kinematic simulation, each of which combines ambient conditions with the effects of solar activity [1-5]. The solar magnetograms and the global photospheric

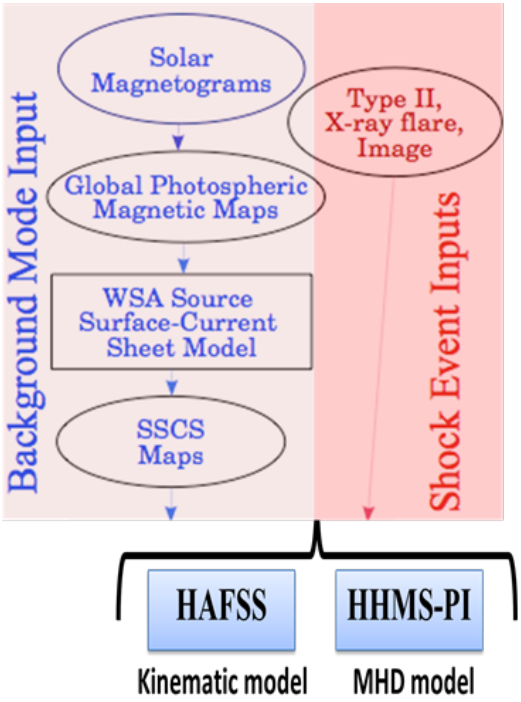


**Figure 2a.**

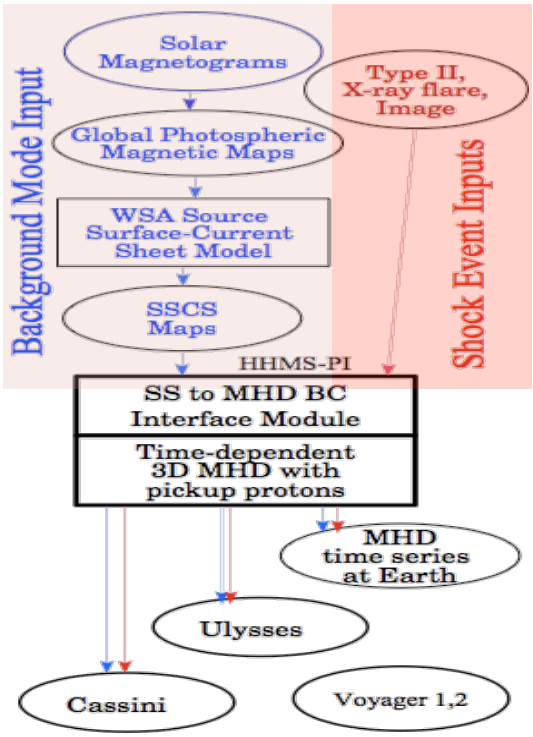


**Figure 2b.**

**Figure 2.** Descriptions of our two three-dimensional (3D) time-dependent HAFSS and HHMS-PI simulations shown in Figure 2a. A more detailed description of our magnetohydrodynamic HHMS-PI simulation is shown in Figure 2b.

magnetic maps are obtained from observations at the Wilcox Solar Observatory (WSO). The blue paths on the left (Figures 2a and 2b) indicate the background or ambient solar and solar wind conditions. The red paths on the right (Figures 2a and 2b) indicate the solar events. It is not appropriate or sufficient to launch a solar event(s) (on the right in Figure 2) without putting it in the context of the ambient or background solar and solar wind conditions (on the left in Figures 2a or 2b).

Figure 2b (the figure on the right) indicates some of the details associated with HHMS-PI, our 3D time-dependent MHD model. For example, HHMS-PI includes the effects of the Local Interstellar Medium (LISM) neutral hydrogen ($N_H$) flowing into the heliosphere and creating pickup protons (PUPs). This can give rise to solar wind heating, and/or slowing. A number of models for heating, turbulence, and other phenomena can be implemented and evaluated through model inter-comparisons and model comparisons with data. In their current forms both HHMS-PI and HAFSS propagate the ambient solar wind and shocks and other features out into an unbounded heliosphere. That is, there is no allowance made for the effects of the termination shock (TS) or for propagation, etc. beyond the TS in the heliosheath (HS). Similarly there are no allowances made for propagation beyond the heliopause (HP) into the LISM. Based on these omissions we assumed that in their present form our two models would not be appropriate for predicting phenomena beyond the TS. To our surprise, we found that beyond the TS the time series simulations predicted by our models were predicting an earlier arrival of

an event or phenomenon compared to that measured in the Voyager 1 (V1) or Voyager 2 (V2) data. This early onset was expected since beyond the TS one assumes that there is a slowing (and heating) of the solar wind.

In using our models and comparing their simulations with spacecraft data we emphasize the importance of quantitative comparisons, correlation coefficients, and/or skill scores, etc. between our simulations and the data rather than only using graphs or cartoons to show the propagation of events. Often the time profile in our simulations agrees well (e.g., highly correlates) with the measured data if one time shifts the measurements to an earlier time. The magnitude of the time shift often is useful in analyzing the underlying physical processes.

## 2. HHMS-PI Simulation of Halloween 2003 Events

Table 1 shows the HHMS-PI shock event inputs from October and November 2003. These inputs are the values that were used in our HHMS-PI simulations as described above in the Introduction in connection with the right sides of Figures 2a and 2b.

**Table 1.** Shock parameters after adjusting for time of arrival at both ACE and Ulysses

| date | time | doy | lat | lon | rad | shSpd | tau | FF |
|---|---|---|---|---|---|---|---|---|
| 2003-10-19 | 16:50 | (292.701) | 5 | -56.0 | 102.0 | 519.6 | 1.33 | 507 |
| 2003-10-21 | 03:47 | (294.158) | -10 | -90.0 | 100.0 | 517.0 | 0.67 | 508 |
| 2003-10-22 | 09:38 | (295.401) | -2 | -22.0 | 100.0 | 781.5 | 3.00 | 509 |
| 2003-10-23 | 08:27 | (296.352) | -21 | -88.0 | 108.0 | 1276.0 | 1.50 | 510 |
| 2003-10-25 | 04:15 | (298.177) | -15 | -43.0 | 120.0 | 530.0 | 2.00 | 511 |
| 2003-10-26 | 06:17 | (299.262) | -18 | -43.0 | 120.0 | 574.1 | 3.00 | 512 |
| 2003-10-26 | 17:35 | (299.733) | 5 | 32.6 | 70.2 | 1027.0 | 3.50 | 513 |
| 2003-10-28 | 11:02 | (301.460) | -16 | -8.0 | 120.0 | 1951.0 | 3.00 | 514 |
| 2003-10-29 | 20:44 | (302.864) | -14 | 1.0 | 123.0 | 1612.4 | 1.50 | 515 |
| 2003-11-01 | 22:34 | (305.940) | -10 | 61.0 | 120.0 | 820.9 | 1.00 | 516 |
| 2003-11-02 | 17:14 | (306.718) | -14 | 82.5 | 158.0 | 1791.4 | 1.00 | 517 |
| 2003-11-03 | 01:24 | (307.058) | 10 | 85.0 | 100.0 | 725.0 | 1.75 | 518 |
| 2003-11-03 | 09:56 | (307.414) | 8 | 77.0 | 120.0 | 1131.3 | 1.50 | 519 |
| 2003-11-04 | 19:43 | (308.822) | -19 | 78.8 | 102.0 | 1580.7 | 1.50 | 520 |
| 2003-11-07 | 15:54 | (311.663) | -18 | 120.0 | 100.0 | 1682.7 | 2.00 | 520.2 |
| 2003-11-11 | 13:35 | (315.566) | -3 | 88.8 | 93.7 | 807.0 | 3.00 | 521 |
| 2003-11-13 | 09:24 | (317.392) | 1 | -90.0 | 101.0 | 718.5 | 3.00 | 522 |
| 2003-11-17 | 09:17 | (321.387) | -1 | -33.0 | 100.0 | 547.0 | 2.00 | 523 |
| 2003-11-18 | 07:47 | (322.324) | 0 | -18.0 | 221.1 | 918.4 | 3.00 | 524 |
| 2003-11-20 | 07:47 | (324.324) | 1 | 14.0 | 104.9 | 997.9 | 0.75 | 525 |

Table 1. Date, Time, Day of Year: start time of metric Type II radio burst. Latitude (degrees), Longitude (degrees), Rad: width of shock (degrees). shSpd is Vs (km/s): shock speed input at the Sun from real-time radio and halo/partial halo CME plane-of-sky speed estimates. Tau (hrs): coronal shocks piston driving time above flare site. FF#: real-time "fearless forecast" events. The content of Table 1 is essentially the same as its components in Table 3 [2] and Table 1 [3].

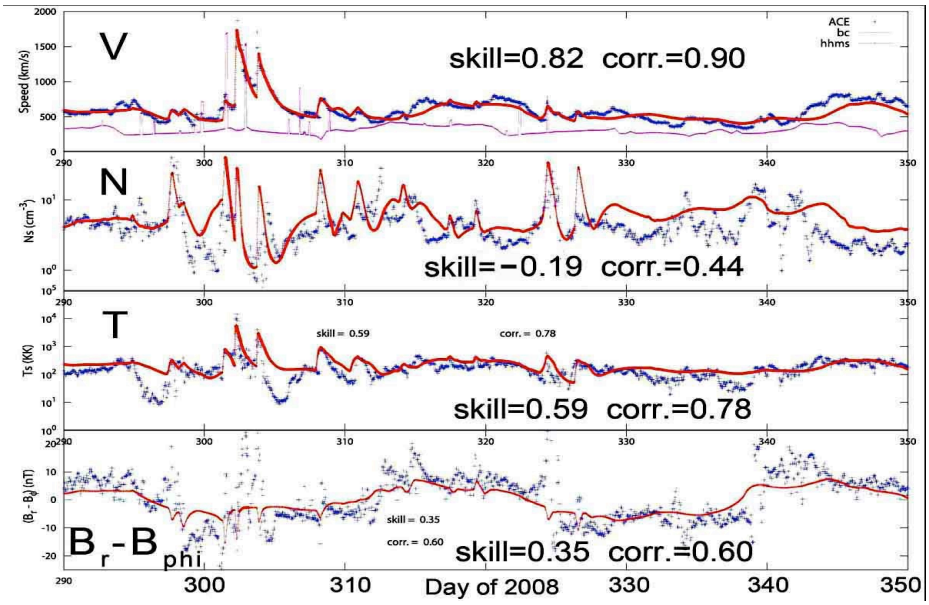


**Figure 3a.** Shows the comparisons [adapted from 2] of the HHMS-PI simulation (red lines) of the Halloween 2003 event with the ACE data [black lines] for the solar wind SWOOPS plasma parameters and magnetic field.

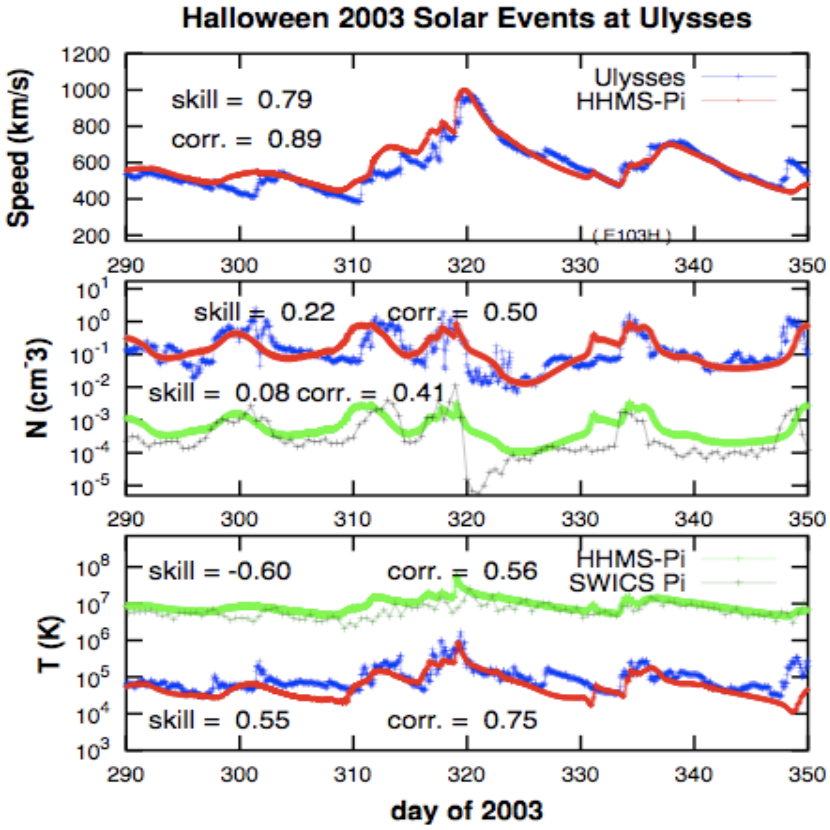


**Figure 3b.** Showing at Ulysses the comparisons [adapted from 3a] for the solar wind plasma parameters with the HHMS-PI simulation (red line). Figure 3b also shows at Ulysses the comparisons of the HHMS-PI simulation (green lines) of the SWICS Pick Up Proton (PUP) density and temperature with these measured PUP parameters (grey lines). These HHMS-PI simulated PUP parameters were predicted by us before the SWICS PUP parameters were available.

Figure 3b is a comparison of the HHMS-PI simulations with Ulysses measurements of the solar wind and PUPs for 60 days in 2003 including quiescent "quiet" undisturbed times and the "disturbed" times associated with the Halloween 2003 events. Shown are the HHMS-PI simulation comparisons at Ulysses with SWOOPS solar wind speed, proton density, and temperature; and with SWICS PUP density and temperature for the "quiet" solar wind both before and after the Halloween events and for the Halloween 2003 events. Note the generally good agreement between the HHMS-PI simulations (in red for the SWOOPS solar wind proton parameters and in green for the SWICS PUP parameters) and the measured plasma speed, densities, and temperatures for both the SWOOPS solar wind protons (in blue) and the measured SWICS PUP density and temperature parameters (in grey) even though at times during the Halloween 2003 event the shape of the plasma distributions is varying greatly as illustrated in [3] in the SWICS spectra (e.g., Days 319.5–320.5) in our Figure 3b.

## 3. HHMS-PI Simulation of Halloween 2003 Events Shows PUPs Slow Down Shock Propagation

The presence of PUPs slows down the propagation of shocks in the solar wind. This is observable even at distances as close to the Sun as ~5 AU. The presence of PUPs can have a significant impact on the propagation of both fast and slower shocks even to these distances. Table 2 and Table 3 summarize some of these results for the Halloween events [1] propagating to Ulysses at ~5.2 AU.

**Table 2.** HHMS-PI Halloween 2003 Transit Speeds at Ulysses Due to Pickup Protons (PUPs).

| Solar Event | Distance (AU) | OBSULY speed km/s | DNH0.1 speed km/s | DNH0.0 speed km/s |
|---|---|---|---|---|
| **514** | **5.24** | **877.4** | **812.1** | **871.0** |
| **517** | **5.25** | **894.2** | **814.7** | **884.1** |
| **520** | **5.25** | **1030.8** | **969.9** | **1048.6** |
| **520.2** | **5.25** | **1239.1** | **1211.6** | **1310.6** |
| **521** | **5.26** | **807.1** | **796.3** | **864.2** |
| **524** | **5.27** | **794.4** | **711.7** | **747.3** |

Table 2 lists from left to right the solar event (Table 1); Distance to Ulysses (AU) (5.24 AU = 783,904,000 km); OBSULY Speed (km/s): Transit speed to Ulysses based on Ulysses data; DNH0.1 Speed (km/s): HHMS-PI Model speed to Ulysses assuming interstellar H density = 0.1 $cm^{-3}$; DNH0.0 Speed (km/s): HHMS-PI Model speed to Ulysses assuming interstellar H density = 0 $cm^{-3}$.

Focusing on Solar Events 520.2 and 521 we can see that the first column on the left in Table 2 shows the numbering of the Solar Events. For Solar Event 520.2 the third column shows that the average speed of the event reaching Ulysses was 1239.1 km/s. The next column (fourth) shows the speed of 1211.6 km/s predicted by the HHMS-PI model resulting from deceleration by pickup from inflowing neutral hydrogen, assuming that the neutral H density was 0.1 $cm^{-3}$. The fifth column shows the predicted speed of 1310.6 km/s from the HHMS-PI Model with INFLOWING NEUTRAL H DENSITY = 0 $cm^{-3}$ (i.e., no deceleration by pickup). Comparing the Ulysses measured shock propagation speed (column 3) with the HHMS-PI predicted speeds from columns 4 and 5 clearly shows that the 1211.6 km/s estimate from the 0.1 $cm^{-3}$ assumption is more appropriate than the estimate from the 0.0 $cm^{-3}$ assumption.

Similarly, for the next Solar Event (521 in column 1), the Ulysses data in column 3 indicates that the shock propagation speed from the Sun to Ulysses was 807.1 km/s, while the 0.1 $cm^{-3}$ assumption provides a speed of 796.3 km/s, which is a little low. However, the 0.0 $cm^{-3}$ assumption predicted a speed of 864.2 km/s, which is quite high compared with the ULYSSES measured speed of 807.1 km/s. Thus for solar event 521, the measured observed Ulysses speed of 807.1 km/s from the Sun to Ulysses, agrees better with the predicted slowing of the solar wind propagation and shock speed by PUPs.

In Table 2 our identifying the solar events of 520.2 and 521 clearly shows the important slowing effects of the PUPs in decelerating the ambient solar wind and shock propagation. This point also is

shown again in Table 3. Looking at Table 3 we find correspondingly that for these same two Solar Events (520.2 and 521) the shifts in the day times agree with the shift in the speeds for these events in Table 2, so that the time to propagate from the Sun to Ulysses was greatly influenced by the PUPs slowing down the plasma and propagation speeds. As shown in the right-hand column, the predicted and actual arrival times for these events agree within about one sixth of a day, or four hours.

Thus, our Halloween 2003 simulations in Tables 2 and 3 show that the PUPs slow large shocks propagating in the solar wind from the Sun to Ulysses at 5.2 AU near the ecliptic plane. We note that others have recognized the importance of how PUPs formed by ionization of the neutral inflowing LISM hydrogen slow large propagating shocks. For example, in 2001, Zank et al. [6] used a 1-D MHD model that included PUP phenomena and interactions of large propagating shocks to predict a qualitatively similar deceleration for the propagation of the July 2000 Bastille Day solar events.

NASA has recently released some press announcements showing some cartoon graphics of the solar wind and shocks flowing from the Sun toward Pluto and the New Horizons spacecraft. We and others have noticed the multiple errors in these NASA cartoons since they exhibit implausibly early arrivals of these solar events at New Horizons because they are based on ENLIL computations that do not account for the PUPs slowing down the outward propagating disturbances from the Sun. Hence, the NASA cartoons omit these effects on the outward flow of the solar events toward New Horizons near Pluto. These erroneous associations in the NASA cartoons showing excessively early arrivals of solar events at New Horizons provide evidence of the importance of PUPs, since PUPs were not included in the 3D time-dependent MHD ENLIL model that attempted to predict the propagation of solar event shocks from the sun to New Horizons.

**TABLE 3.** HHMS-PI Shock Arrival Times (and Delays) at Ulysses Due to Pickup Protons (PUPs).

| Solar Event | Solar Event Day | OBSULY Arrival Day | DNH0.1 Arrival Day | DNH0.0 Arrival Day | DNH0.1-DNH0.0 (Days) | OBSULY-Best Pred (Days) |
|---|---|---|---|---|---|---|
| **514** | **301.460** | **311.801** | **312.632** | **311.877*** | **0.755** | **-0.076** |
| **517** | **306.718** | **316.884** | **317.876** | **317.000*** | **0.876** | **-0.116** |
| **520** | **308.822** | **317.641** | **318.194** | **317.491*** | **0.703** | **0.150** |
| **520.2** | **311.664** | **319.000** | **319.167*** | **318.600** | **0.567** | **-0.167** |
| **521** | **315.566** | **326.851** | **327.004*** | **326.105** | **0.899** | **-0.153** |
| **524** | **322.324** | **333.810** | **335.145** | **334.534*** | **0.611** | **-0.724** |

Table 3 lists from left to right the solar event (Table 1); Distance to Ulysses (AU) (5.24 AU = 783,904,000 km); OBSULY Arrival Day: Transit Times to Ulysses based on Ulysses data; DNH0.1 Arrival Day: Transit Times to Ulysses based on HHMS-PI Model with INFLOWING NEUTRAL H DENSITY = 0.1 $cm^{-3}$; DNH0.0 Arrival Day: Transit Times to Ulysses based on HHMS-PI Model with INFLOWING NEUTRAL H DENSITY = 0 $cm^{-3}$; asterisks in the DNH0.1 and DNH0.0 columns indicate for each event which model gave the best prediction, which is used in the right-hand column.

## 4. HHMS-PI Simulations of Halloween 2003 Events Show They Can't Unambiguously Help Us Determine the HCS Tilt Orientations at V1 and V2 in 2004

The orange lines in Figure 4 show the vertical displacement of the Heliospheric Current Sheet (HCS) for V1 and V2 in 2004, as estimated by taking data from the Wilcox Solar Observatory (WSO) and allowing for possible propagation delays to the spacecraft by shifting the WSO data 270 days (WSO + 270 days: Figure 4a) and 360 days (WSO + 360 days: Figure 4b). In these panels the V1 Trajectory is shown as a red horizontal line at 31 degrees North in heliographic inertial (HGI) coordinates, meaning that the spacecraft remained at this latitude without significant change as it travelled outward a distance of about 3.5 AU during this year, since the latitudinal component of its velocity vector was

close to 31 degrees North. Similarly, the V2 trajectory is shown as an almost exactly horizontal blue line at ~ 26 degrees South HGI, since it travelled outward about 3 AU during this year, but its latitude changed by only about 0.25 degrees, which is too small to be visible on this scale.

In each panel, the asterisks (in colours matching the corresponding trajectory lines) show the sector boundaries found in the magnetometer data from the respective spacecraft during the times that each was observing phenomena that appear to be the shock and other disturbances generated by the Halloween 2003 flares [4,5] (and during some of the previous period in the case of V2, since the plasma instrument on V2 is still working, while the V1 plasma instrument failed in 1980; on the other hand, currently the V2 magnetometer data are not publicly available from June 18, 2004 (day 170) to the end of the year, though the available data resume at the beginning of 2005). At the bottom of the figures the red vertical arrows sticking up on each figure indicate the times of the two forward shocks at V2 (Day 119, 2004) and V1 (Day 209, 2004).

As can be seen from these panels, these magnetometer data do not provide strong evidence for identifying the propagation delay more definitely than the previously estimated range of 270 to 360 days. Thus, until the V2 magnetometer data for the last half of 2004 become available, we are unable to determine what delay of the HCS results from the WSO data (which, as noted in the Introduction, are the fundamental inputs to our modelling computations) may be better suited for analyses of the effects of the Halloween 2003 events and the periods before and after, as observed at the Voyagers.

We should note that when additional V2 magnetometer data become available either in 2004 or later (such as in 2013, 2014, etc.) we also should be able to make some additional comparable plots to those in Figures 4a and 4b that may allow us to distinguish the various sector boundaries in the V1 and V2 magnetometer data and their respective relations to the WSO HCS tilt angles. This may provide a great deal of help not only for understanding how well the estimated WSO tilt angles predict when the spacecraft should be crossing the current sheet and hence observing sector boundaries, but it may provide useful comparisons with the models described in the previous sections and also may supply important information about the transport of the magnetic field within the heliosheath and perhaps eventually in the LISM.

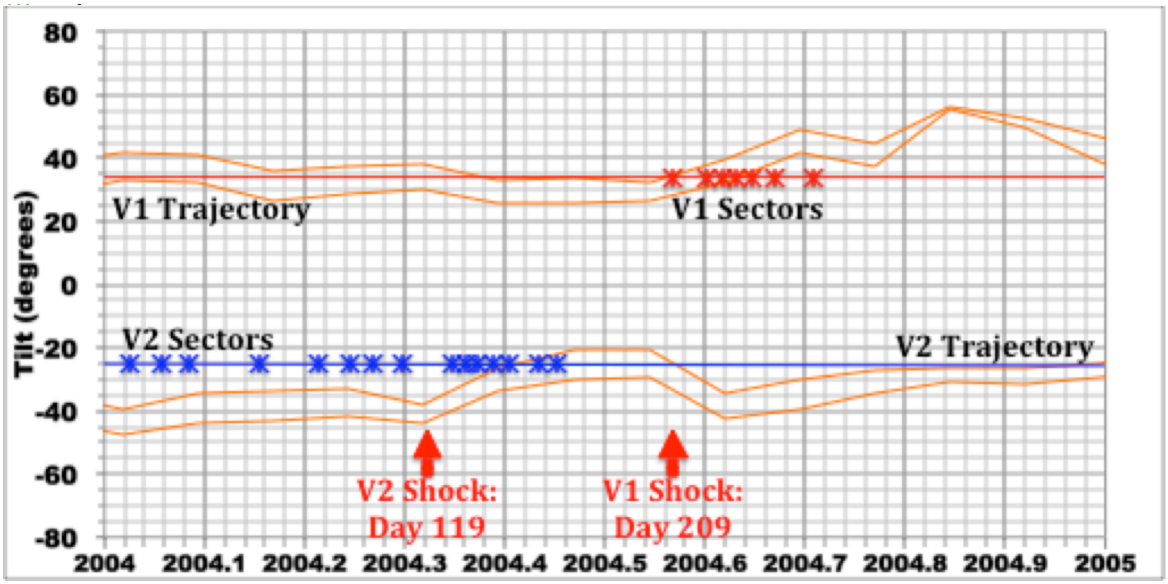


**Figure 4a**. Halloween 2003 WSO HCS Tilt Angles + 270 days with V2 & V1 Sector Boundaries.

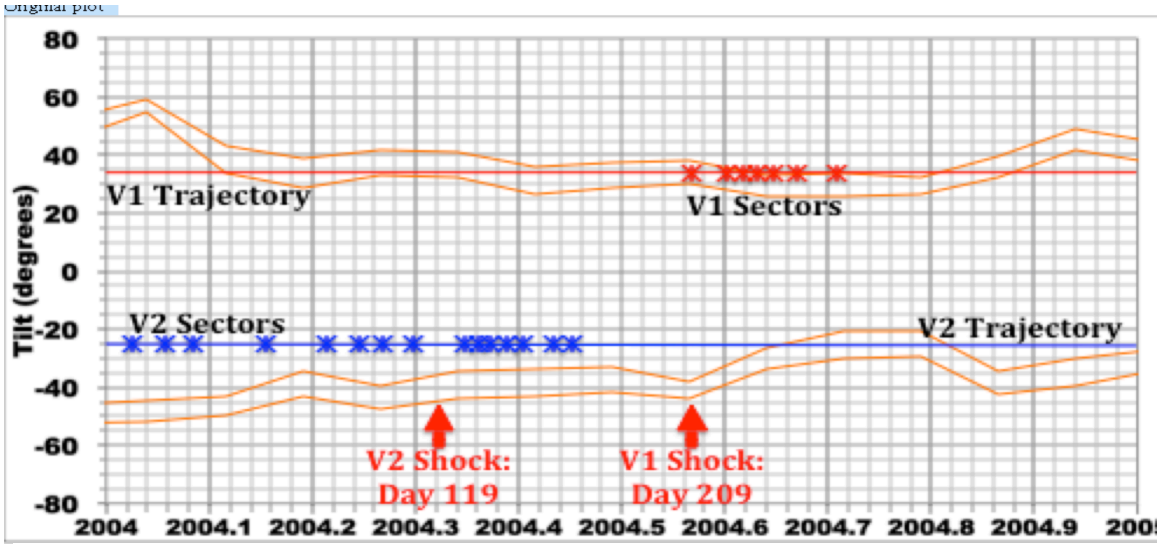


**Figure 4b**. Halloween 2003 WSO HCS Tilt Angles + 360 days with V2 & V1 Sector Boundaries.

## 5. The Importance of Geometry in the Simulations: the Locations of Solar Events and the Spacecraft

Figures 5a, 5b, and 5c indicate the locations of the flares at the Sun and the positions of the various spacecraft for, respectively, the Oct./Nov. 2003 solar events, the March 2012 solar events, and the July 2012 solar events, as if viewed from a point far above the solar north pole. In each of these plots the orange round dot in the center represents the Sun and the adjacent red asterisk shows the location of the flare that occurred at the time given at the top of the plot. As indicated by the labels and abbreviations, the positions of the various spacecraft are shown in each plot with a logarithmic scale of radial distance from the Sun. Thus, the blue round dots at 1 AU represent the positions of Earth (with ACE at the $L_1$ Lagrangian point about 1.5 million km radially sunward of the Earth at all times), and for the 2012 events STEREO A and B (SA and SB) also are located at 1 AU with ~120 degrees of longitude separating Earth, SA, and SB. For the Oct/Nov 2003 events the Ulysses spacecraft are at the green squares about 5.2 AU from the Sun; and the much more distant labelled green squares show the respective V1 and V2 spacecraft locations for all three series of these solar events. The projections onto the ecliptic plane in these figures do not indicate that in these years V1 was about 30 degrees North of the ecliptic plane, while V2 was about 26 degrees South, with trajectories taking them respectively to gradually increasing North and South latitudes.

In each figure the various spacecraft are shown at the positions where they were at the times of the flares. The shocks, CMEs, and energetic particle effects of the flares reached the spacecraft after propagation delays that ranged from hours or days for the spacecraft at 1 AU to a year or more for V1 and V2 far beyond the outer radius of the Kuiper Belt. However, in each case the velocities of the spacecraft were small enough, relative to their distances from the Sun, that they did not move significantly on the scales of these figures during their respective propagation delays, so that it is possible in each figure to extrapolate from the location of each flare to the location of each spacecraft in interpreting the observations, even though the spacecraft closer to the Sun moved significantly during the propagation delays to the more distant spacecraft. Thus, in each figure, when they detected the shocks the spacecraft near the Earth, the STEREO spacecraft, and Ulysses were respectively where they are shown, even though they all moved significantly during the subsequent months that the shocks took to reach the Voyagers, and because of the logarithmic distance scale the Voyagers are in nearly the same positions in all the figures, despite the years that elapsed from late 2003 to the middle of 2012.

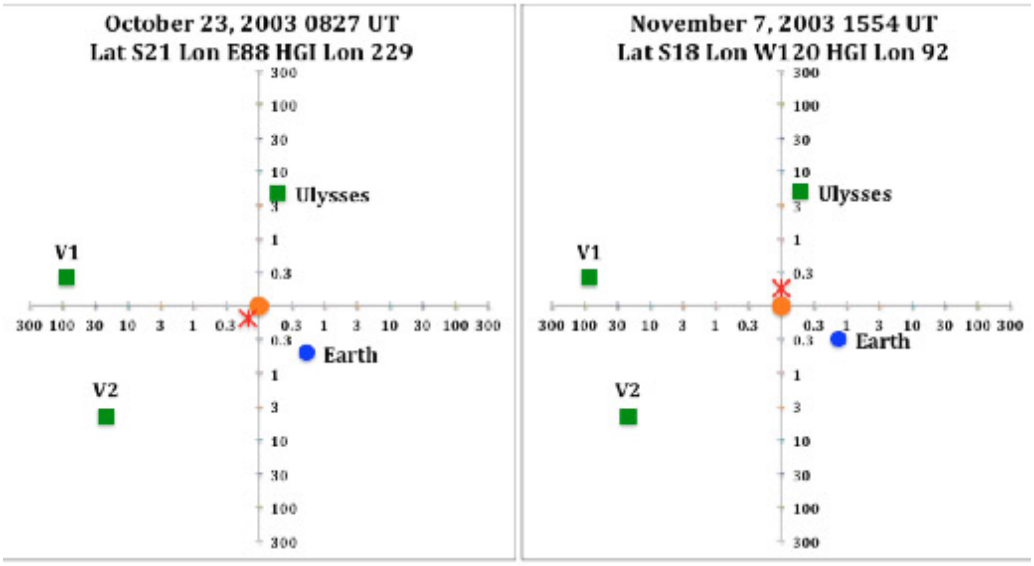


**Figure 5a.** October-November (Halloween) 2003 Solar Events.

The left panel of Figure 5a shows that the Oct. 23, 2003 solar event was located on the side of the Sun facing V2 at ~East 88 degrees as viewed from Earth, or a HGI longitude of 229 degrees. Note that Ulysses at ~5.2 AU was about 140 degrees from this flare. By contrast, the right panel of Figure 5a indicates that the Nov. 7 flare was located about 120 degrees west of Earth at HGI longitude 92 degrees, in the direction of the Ulysses spacecraft.

Thus, the Oct. 23 flare and several that occurred in the same active region in the next few days were all well observed from the Earth, but since the Nov. 7 flare occurred after the active region had rotated over the west limb of the Sun as viewed from the Earth, its importance was not recognized until the Ulysses experimenters sought an explanation for the unusually high solar wind speed of 993 km/s observed on Nov. 15, after which evidence of the flare was found in coronagraph observations. (This is why this event had to be added *post facto* as event 520.2 to the master list of events used to prepare Tables 1, 2, and 3.)

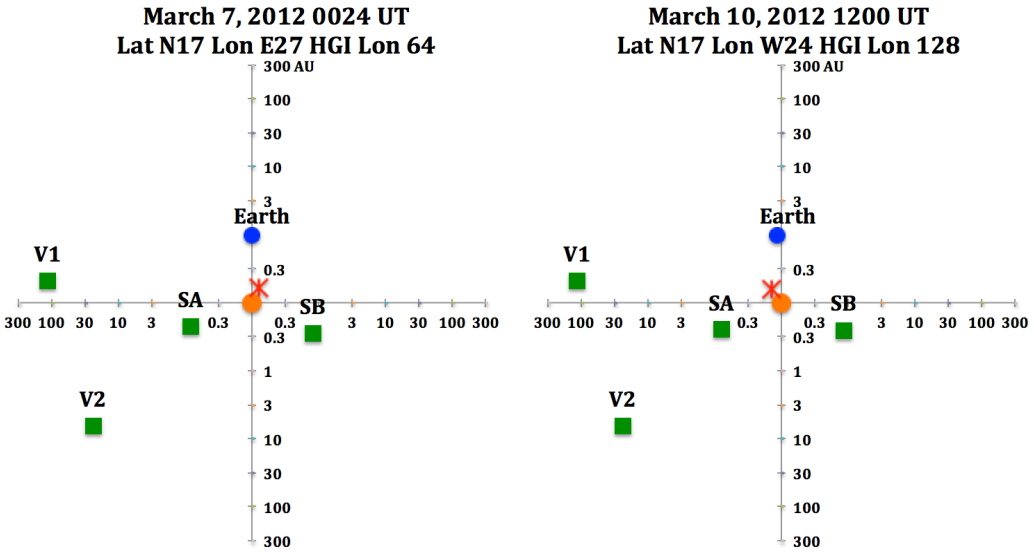


**Figure 5b.** March 2012 Solar Events.

The figures also show that both the Oct. 23 and the Nov. 7 flares were well located for their shocks to be observed by the Voyagers, although because of the rotation of the active region some of the flares during intermediate days, though well located for observations from Earth, were at unfavourable locations to be detected after propagation by the Voyagers. As described in Table 4 below, events associated with this period of major flares were detected at both V1 and V2 in 2004. However, owing to interaction region merging over the long distance to the Voyagers (we have previously reported [4] an analysis of the merged interaction regions (MIRs) observed in the V2 data in April and May, 2004), it is not possible to identify the contributions of the individual flares to the phenomena observed at the Voyagers.

As Figure 5b shows, the March 7, 2012 flare was located in a good position to be observed at the Earth and STEREO B, but was nearly on the opposite side of the Sun from STEREO A and V2, while the March 10, 2012 flare was nearly on the opposite side of the Sun from STEREO B, but was well positioned for the Earth, STEREO A, and the Voyagers, especially V1, since the flare was about 50 degrees east of V1.

This event may be responsible for important phenomena observed by Voyager 1 in April 2013. As these two March 2012 flares were both located on the Sun at a North latitude of 17 degrees and V1 was located near North 30 degrees, V1 was in a particularly favourable position to observe the effects of the March 10 flare, with possible contributions from the March 7 flare and lesser ones in the previous few days. In particular, the shocks and other phenomena generated by this group of flares are

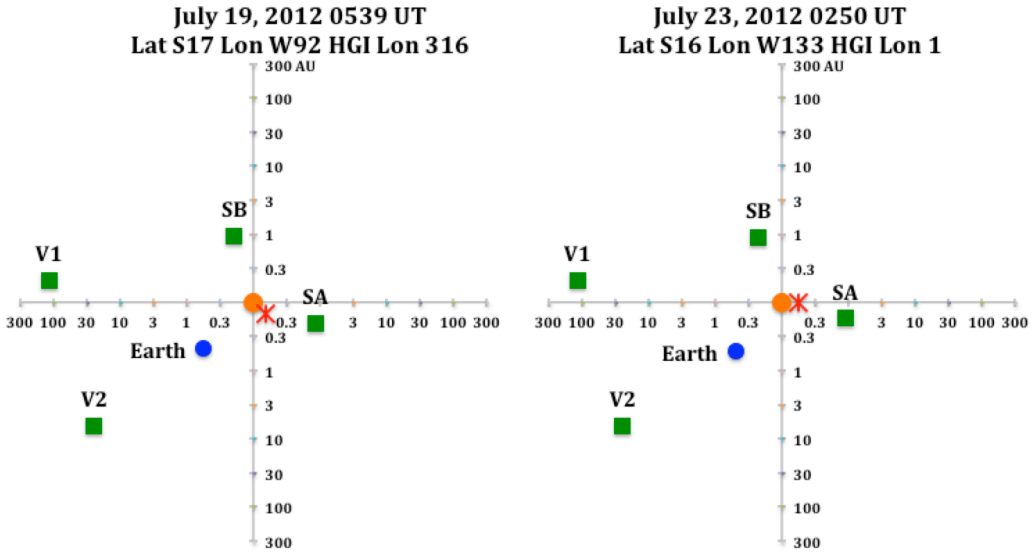


**Figure 5c.** July 2012 Solar Events.

believed to be the source of the 3 kHz signals detected by the V1 plasma wave system (PWS) that provided conclusive evidence (by corresponding to a plasma electron density of about 0.08 $cm^{-3}$) that the jump in the cosmic ray count rate observed by the Voyager instruments in August 2012 did in fact mark the spacecraft's transit through the heliopause (HP) and entry into the local interstellar medium (LISM).

Many colleagues likened the July 23, 2012 solar event (on the right side of Figure 5c) to the Carrington 1859 solar event. The July 23, flare occurred at a latitude of south ~ 26 degrees and at a HGI longitude of 1 degree, so V2 was more favourably located in latitude than V1 to observe the effects of this flare, but the large longitude separation diminished the effect.

As the right panel of Figure 5c shows [5], the July 23 flare occurred when its active region had rotated well beyond the west limb of the Sun, as viewed from the Earth, so the world escaped what might have been an international technological catastrophe if the shock from this flare had caused a Carrington-class geomagnetic storm. As it was, the effects at the Earth were small, while STEREO A,

being almost radially aligned with the flare, was subjected to solar wind speeds that exceeded the measurement range of its instruments. Elsewhere [5] we have estimated the peak speed at STEREO A of the plasma in the CME from this event at nearly 3000 km/s, but this is based on the HAFSS kinematic simulation, for a period during which the STEREO experimenters have no usable data from their solar wind instrument.

However, in view of the extraordinary power of this event, it is plausible to associate it with phenomena observed at V1 in 2014, even though, as the figure shows, V1 was nearly on the opposite side of the Sun from this flare. In particular, on May 20, 2014, the V1 PWS began to detect another 3 kHz plasma wave event similar to the one in April and May, 2013, that we attributed above to a shock associated with the March 2012 flare events, so it seems likely that this plasma wave event also resulted from a flare shock, for which the July flare events, especially the July 23 flare, are the most likely source. We attribute the low average propagation speed to V1 to the unfavourable location of the spacecraft, while a higher average propagation speed to V2 (both shown below in Table 4) is probably due to the more favourable location with respect to this spacecraft of both this flare and the July 19 flare.

Figures 5a, 5b, and 5c all illustrate the advantages of looking at pairs of plots for the periods of powerful flares to see how the geometric relationships between the flare locations and the spacecraft locations aid in understanding the propagation of the shocks and CMEs generated by these solar events. Table 4 in the next section presents quantitative ranges for the delay times and average transit speeds of the shocks from the flares that produced them to when the Voyagers observed them.

## 6. Shock Delays and Average Transit Speeds

Table 4 summarizes the shock transits from the Sun to V2 and to V1 for the solar flare events of Oct./Nov. (Halloween) 2003; March 2012; and July 2012. All of the dates, delays, and transit speeds in Table 4 are based strictly on the times of the events at the Sun and the times of the measurements of the events at the spacecraft that have been identified as corresponding to the respective solar flares, without referring to any outside models not connected with these measurements.

| **Halloween 2003 Flare Events** | **V2 observations** | **V1 observations** |
|---|---|---|
| Delay (days) Apr. 28, 2004 at V2<br>Jul. 27, 2004 at V1 | 173-188 | 263-278 |
| Average transit speed (km/s) | 674-732 | 577-610 |
| **March 2012 Flare Events** | | |
| Delay (days) Apr. 18, 2013 at V2<br>Apr. 25, 2013 at V1 | 404-407 | 411-414 |
| Average transit speed (km/s) | 432-435 | 518-522 |
| **July 2012 Flare Events** | | |
| Delay (days) Aug. 30, 2013 at V2<br>May 20, 2014 at V1 | 403-407 | 666-670 |
| Average transit speed (km/s) | 436-441 | 330-332 |

**Table 4.** Shock Summaries and Comparisons for Three Solar Events: October/November (Halloween) 2003 solar events; the March 2012 solar events; and the July 2012 solar events.

This point is important. We decided to use only dates, measurements, etc. that were obtained from solar observations and in spacecraft data when those numbers are beyond reproach. Thus, if the measured shock speed or its related values can't be verified, we don't want to consider using them. Thus, any *a priori* methods or numbers based on other types of analyses are not accepted.

In Table 4 the first (top) columns indicate for the Halloween (Oct./Nov) 2003 solar events that the start date of the first event reaching Voyager 2 (V2) was on April 28 (Day 119), 2004. This corresponds to a delay time from the Sun to V2 of 173-188 days. The second top column indicates that these Halloween solar events reached V1 on July 27 (Day 209), 2004. This corresponds to a delay time from the Sun to V1 of 263-278 days. The Average Transit Speed delay time (see bottom row for the Halloween events in Table 4) for these events were for V2: 264-732 km/s; and for V1: 577-610

km/s. Similar numbers are shown in Table 4 for the March 2012 and July 2012 solar events and for their corresponding measured phenomena at V2 and V1.

For this Halloween 2003 solar event, since all of the final shocks reached V2 and V1 when these spacecraft were both still in the heliosphere, this does not imply any simplified imaging or backward projections of these events. However, the shocks from the March 2012 and the July 2012 solar events reached V2 and V1 after these two spacecraft had travelled beyond the termination shock (TS) and into the heliosheath (HS). In addition, the solar shocks from the July 2012 solar event appear to have reached V1 after V1 had left the HS and had entered the Local Interstellar Medium (LISM), since V1 crossed the heliopause (HP) on August 25, 2012. Thus, any correct modeling of these March 2012 and July 2012 solar events would have to take account of the propagation of these events in the heliosheath. Furthermore, for the July 2012 solar events of which the effects appear to have reached V1 in 2014, since the spacecraft had already crossed the HP in August of 2012 the modeling would also have to estimate propagation in the LISM. It is not obvious now what would be the correct modeling formulas for these events when the spacecraft are in the HS and/or in the LISM. Thus, we decided to base our current estimates only on the data presently available. In the future when more V2 and V1 data are available and when V2 crosses the HP, we will plan to employ these newly available data for future estimates and calculations.

## 7. Summary

We presented some examples that show the Sun is a dynamic influence in the heliosphere, the HS, and the LISM. Our models and data comparisons provide key insights. We prefer to use measured quantitative data at the Sun and at the spacecraft rather than relying on inferred numerical values at these various locations. We employ our two 3D time-dependent models that start near the Sun (2.5 Rs) where they input solar background and solar event boundary conditions derived from solar observatory magnetograms. These two 3D time-dependent models simulate the propagation of shocks, other specific features, and the background solar wind throughout the heliosphere. The Hybrid Heliospheric Modeling System with Pickup Protons (HHMS-PI) is a 3D time-dependent Magnetohydrodynamic (MHD) simulation. HAFSS (HAF Solar Surface) is a 3D time-dependent kinematic simulation. Our models and data comparisons indicate that quantitative solar effects are seen in the heliosphere, the HS, and the LISM in in-situ spacecraft measurements of plasma, magnetic field, energetic particles, cosmic rays, and plasma waves. There is quantitative agreement (at ACE, Ulysses, V1, V2) with data (e.g., solar wind, IMF, Ulysses SWICS pickup protons (PUPs)). Quantitatively we showed examples of propagating shocks slowed due to PUPs. The 3D locations and measurements of solar events and of their corresponding features at various spacecraft are key to understanding the 3D propagation and timing of shocks, other specific features, and gradients throughout the heliosphere, HS, and LISM.

## 8. References

[1] Intriligator D S, Sun W, et al., 2005, *J. Geophys. Res.,* **110**, A09S10, doi:10.1029/2004JA010939.
[2] Detman T M, Intriligator D S, et al., 2011, *J. Geophys. Res.,* **116**. A03105, doi:10.
1029/2010JA015803.
[3] Intriligator D S, Detman T M, Gloeckler G, et al., 2012, *J. Geophys. Res.,* **117**, A06104,
doi:10.1029/2011JA017424.
[4] Intriligator D S, et al., AGU presentation, 2011.
[5] Intriligator D S, et al., 2015, *J. Geophys. Res.,* **120**, 8267–8280, doi:10.1002/2015JA021406.
[6] Zank G P, et al., 2001, *J. Geophys. Res.,* **106**, A12, 29363-29372, doi: 10.1029/2000JA000401.

## Acknowledgments

We gratefully thank Professor Edward C. Stone, and the ACE and Voyager projects for the vast information we have received. We acknowledge the support of Carmel Research Center, Inc.